ACS OMEGA

http://pubs.acs.org/journal/acsodf

Article

Solubility, Crystallization, and Characterization of Cytidine Sulfate

Fan Leng, Shuyang Zhou, Shushu Li, Mengjie Xu, Keke Zhang, Ting Guo, Tianpeng Chen, and Pengpeng Yang*

Cite This: *ACS Omega* 2023, 8, 25288−25294

Read Online

ACCESS | Metrics & More | Article Recommendations | Supporting Information

ABSTRACT: Cytidine is an important kind of nucleoside that can be applied to drug development and food industry. Cytidine sulfate is one of its popular forms, which is promising as a medicinal intermediate, especially in antiviral and antitumor drugs. Product refining is the key point of industrial development, and crystallization is a significant way of refining. In this work, the solubility of cytidine sulfate in pure water from 278.15 to 328.15 K and in water−ethanol binary solvents at 298.15 K was measured by the UV spectroscopic method. The solubility data were correlated with temperature and solvent composition using the modified Apelblat, van't Hoff, and CNIBS/R-K equations. On this basis, we investigated and compared three crystallization processes, and the coupling method was developed to prepare crystals with a large particle size, concentrated distribution, and high yield and packing density. In addition, the structure and stability of the products were characterized by powder X-ray diffraction, Fourier transform infrared spectroscopy, thermogravimetric analysis, differential scanning calorimetry, and dynamic vapor sorption analysis. It was found that cytidine sulfate has only one crystal form in our research process, and the product of coupling crystallization is stable and favorable for industrial development.

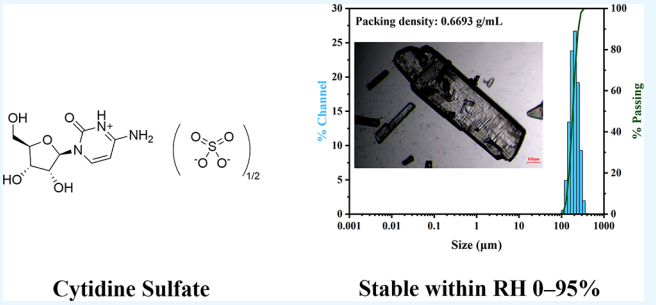

1. INTRODUCTION

Cytidine, known as a kind of nucleoside, is formed by connecting the N-1 position of cytosine to the C-1 position of D-ribose via a β-glycosidic bond. Cytidine is an important component of nucleic acid in an organism. It exists mainly in the form of cytidylic acid, such as cytidine monophosphate (CMP), cytidine diphosphate (CDP), and cytidine triphosphate (CTP), which produces physiological effects in cells. Cytidine is widely used in the development of antiviral and antitumor drugs[1] and is the main material to produce cytarabine, ancitabine, zalcitabine, and other relative drugs. Cytarabine is the first choice for the treatment of acute myeloid leukemia. It is also used in different stages of treatment of other leukemia.[2,3] Ancitabine is converted into cytarabine in the body and acts in a similar fashion. Zalcitabine is one of the approved antiretroviral drugs for the treatment of AIDS in the USA and Europe. It interacts with the catalytic site of the enzyme in HIV as one of the nucleoside reverse transcriptase inhibitors.[4] In addition, Gopalsamuthiram et al.[5] reported a scalable four-step synthesis of molnupiravir, a promising drug candidate for treating COVID-19, from cytidine. With the extensive research and development of antiviral and antitumor drugs, as well as the expansion of studies on its function, the market demand for cytidine is increasing.

At present, biological fermentation is the main method for the industrial production of cytidine.[6] In the process of biological separation, it is common to convert cytidine to cytidine sulfate (Figure 1). The crystallization of cytidine sulfate is of great significance in removing trace impurities and providing a material with high quality for downstream handling. High-quality cytidine sulfate has good application prospects in the field of medicinal intermediates.

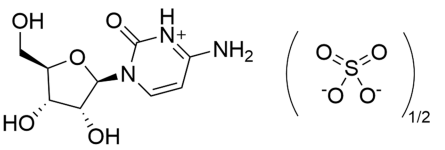

Figure 1. Molecular structure of cytidine sulfate.

Crystallization is widely used in the chemical industry for purification, stable solid form screening, or particle size control.[7] To our knowledge, there are few reports on the solid−liquid equilibrium and crystallization process of cytidine sulfate.

In this work, we investigated the basic thermodynamic data of cytidine sulfate and the effect of the crystallization method

Received: April 13, 2023
Accepted: May 10, 2023
Published: July 7, 2023

on the quality of products, aiming to develop a green and efficient crystallization process for industrial production. On this basis, the structure and stability of the products were characterized.

2. EXPERIMENTAL SECTION

2.1. Materials. Cytidine sulfate was prepared in our laboratory by salt-forming crystallization, with a purity of greater than 99% in mass fraction and approximately 100% in HPLC. The PXRD pattern and FTIR spectrum of the raw material are shown in Figure S1. Analytical-grade ethanol was purchased from Wuxi City Yasheng Chemical Co. Deionized water was generated by an ultrapure water system (YPYD Co., China).

2.2. Solubility Measurement. The solubility of cytidine sulfate in pure water from 278.15 to 328.15 K and in water−ethanol binary solvents at 298.15 K was measured by the UV spectroscopic method under atmospheric pressure.[8,9] The maximum absorption wavelength of cytidine sulfate was located around 274 nm by full-wavelength scanning. The calibration curve of cytidine sulfate was measured at room temperature and atmospheric pressure.

For each measurement, a certain amount of solvent and an excess mass of cytidine sulfate were added to a sealed bottle. The slurry was kept stirring for 6 h and then kept still for 4 h, ensuring to reach fully solid−liquid equilibrium. The temperature was controlled to be constant by circulating water (CK-4005GD, scientz, China) with an accuracy of ±0.05 K in the whole process. Approximately 3 mL of an upper clear solution was filtered and injected into a centrifuge tube using a preheated filter (0.22 μm, PES) and an injector for weighing and dilution. An electronic analytical balance (HZY-224/323, HZ) with an accuracy of ±0.0001 g was used to measure all the masses. The filtrate was diluted to a concentration that was within the linearity range for UV detection. Each of the experiments was conducted three times, and the mean value was used to calculate the solubility.

Equation 1 was applied to calculate the mole fraction solubility of the solute in pure water and in different proportions of water−ethanol binary solvents. Equation 2 was applied to define the mole fraction of ethanol in binary mixed solvents.

$$x_1 = \frac{m_1/M_1}{m_1/M_1 + m_2/M_2 + m_3/M_3} \quad (1)$$

$$x_2 = \frac{m_2/M_2}{m_2/M_2 + m_3/M_3} \quad (2)$$

where x_1 represents the mole fraction solubility of cytidine sulfate; x_2 is the mole fraction of ethanol in binary solvent mixtures; m_1, m_2, and m_3 represent the masses of cytidine sulfate, ethanol, and water, respectively; M_1, M_2, and M_3 represent the molecular weights of the relevant solute and solvents, respectively.[7,10]

2.3. Crystallization of Cytidine Sulfate. *2.3.1. Cooling Crystallization.* 17.5 g of cytidine sulfate powder was employed to prepare 70 mL of aqueous solution in a 100 mL jacketed crystallizer, in which the temperature was controlled by circulating water. The solution was heated to 328.15 K and equilibrated for 1 h with stirring controlled by an overhead stirrer (EUROSTAR 20 digital, IKA, Germany). The system was then cooled down to 288.15 K at the rate of 0.5 or 1.0 K/min for crystallization and kept stirring at 288.15 K for 2 h. The crystal product was separated from the slurry by filtration and drying.

2.3.2. Antisolvent Crystallization. Ethanol was chosen to be the antisolvent. 12 g of cytidine sulfate powder was employed to prepare 100 mL of aqueous solution in a 500 mL jacketed crystallizer. The solution was kept at 298.15 K for 1 h with stirring. Then, 300 mL of ethanol was pumped into the system at the rate of 0.5 or 1.0 mL/min by a peristaltic pump (BT100LC, Baoding Chuang Rui, China). The crystals were stabilized for 2 h after the feeding was completed. The product was collected by filtration, washing, and drying.

2.3.3. Cooling−Antisolvent Coupling Crystallization. 17.5 g of cytidine sulfate powder was employed to prepare 70 mL of aqueous solution in a 250 mL jacketed crystallizer. The solution was heated to 328.15 K and equilibrated for 1 h with stirring. The system was then cooled down to the cloud point (317.15 ± 2 K) at the rate of 0.2 K/min and kept at the temperature for 40 min, during which the crystals increased in quantity. Then, the system was continued cooling to 288.15 K at the same rate. After the cooling, 140 mL of ethanol was pumped into the system at the rate of 1.0 mL/min. Finally, the crystals were stabilized for 2 h and collected by filtration, washing, and drying.

2.4. Product Characterization. *2.4.1. Particle Size Distribution and Packing Density.* The particle size distribution of the products was determined by the wet measurement using a particle size analyzer (Mastersizer 3000, Malvern Panalytical, U.K.). Ethanol was used as the carrier solvent.

2.4.2. Optical Microscopy. Polarizing microscope (Mshot MP41, MSHOT, China) images were taken to observe the shape and size of the crystals.

2.4.3. Fourier Transform Infrared Spectroscopy. Infrared spectra of the products were obtained by an FTIR spectrometer (Nicolet iS5, Thermo Scientific) with an ATR attachment in the wavenumber range of 4000−625 cm^{-1}, with a resolution of 4 cm^{-1} under ambient conditions.

2.4.4. Powder X-ray Diffraction. PXRD analyses of the products were performed with an intelligent X-ray diffractometer (Empyrean, Malvern Panalytical, U.K.) at room temperature. The measurement conditions were as follows: Cu Kα radiation (λ = 1.5406 Å); scan range, 5−40° 2θ; step size, 0.0260° 2θ; scan step time, 45.900 s.

2.4.5. Thermogravimetric Analysis and Differential Scanning Calorimetry. Thermogravimetric analysis (TGA) and differential scanning calorimetry (DSC) were carried out on a simultaneous thermal analyzer (TGA-DSC/HT/1600, Mettler-Toledo, Switzerland) to characterize the thermal behaviors of the products. Approximately 5 mg of each sample was added to an aluminum crucible and heated at the rate of 10 K/min from 30 to 500 °C under a 50 mL/min nitrogen flow. STARe thermal analysis software was used to process data.

2.4.6. Dynamic Vapor Sorption Analysis. Dynamic vapor sorption (DVS) analysis was conducted on a multipurpose thermal analyzer (TGA Q5000 V3.17 Build 265, TA Instruments). Approximately 50 mg of each sample was equilibrated and data were marked sequentially at the relative humidity of 0−5−20−35−50−65−80−95−80−65−50−35−20−5%. The temperature was set to 25 °C. The balance gas was 10 mL/min of nitrogen, and the humidity gas was 200 mL/min of nitrogen. The software Universal V4.5 A was used

https://doi.org/10.1021/acsomega.3c02501
ACS Omega 2023, 8, 25288−25294

for analysis. The mass change calculated by eq 3 was used to assess the humidity stability of the products.

$$\text{mass change} = \frac{m - m_0}{m_0} \times 100\% \quad (3)$$

where m_0 represents the initial mass of the product and m represents the mass of the product obtained by real-time measurement during the experiment.

3. RESULTS AND DISCUSSION

3.1. Solubility Data and Model Correlation. The solubility data of cytidine sulfate in pure water within 278.15−328.15 K are listed in Table S1. The relation between mole fraction solubility and temperature was correlated by the modified Apelblat equation as expressed in eq 4.[11,12] The calculated Apelblat solubility data (x^{Apelblat}) are also given in Table S1.

$$\ln x_1 = A + \frac{B}{T} + C \ln T \quad (4)$$

where x_1 is the mole fraction solubility of cytidine sulfate; T is the absolute temperature (K) at which the solid−liquid equilibrium was reached; and A, B, and C are empirical parameters fitted by the solubility data and equilibrium temperature.

The experimental solubility data and fitting curve are shown in Figure 2. The solubility of cytidine sulfate increases

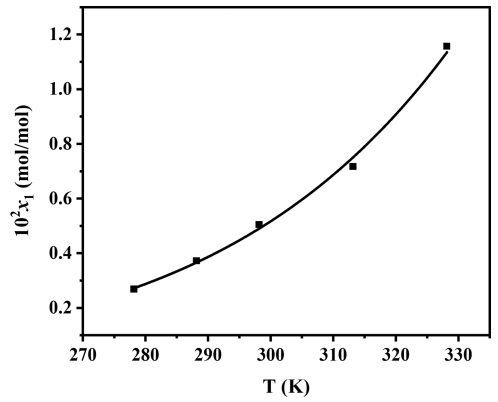

Figure 2. Mole fraction solubility of cytidine sulfate in pure water correlated by the modified Apelblat equation.

obviously as the temperature rises in pure water, indicating that cooling may be taken as a feasible method for crystallization. Yet, the solubility was found to be still favorable at 278.15 K, approximately 87.3 g per liter of water, which leads to the relatively low yield during batch crystallization.

The values of A, B, C, and R^2 and the root-mean-square deviations (RMSD) are listed in Table S2. As is shown in Figure 2 and Table S2, it proved that the experimental solubility data fits well with the modified Apelblat equation.

Thermodynamic parameters of the dissolution process were fitted and calculated by the van't Hoff equation as expressed in eq 5.[13,14]

$$\ln x_1 = -\frac{\Delta H_d}{RT} + \frac{\Delta S_d}{R} \quad (5)$$

where ΔH_d and ΔS_d are the dissolution enthalpy and entropy, respectively.[15,16] Using the natural logarithm of the solubility of cytidine sulfate ($\ln x_1$) versus $1/T$ plot, as shown in Figure 3, ΔH_d and ΔS_d were obtained from the slope and the intercept,

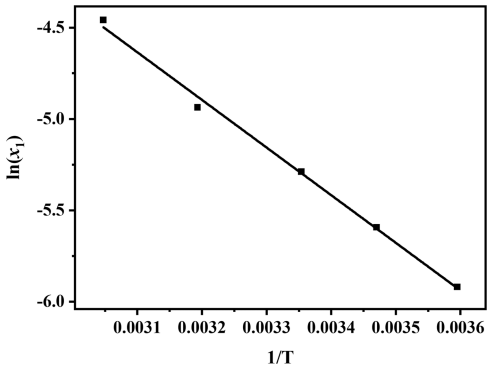

Figure 3. Mole fraction solubility of cytidine sulfate in pure water correlated by the van't Hoff equation.

respectively.[17] Besides, in order to calculate the Gibbs free energy (ΔG_d), the relative contributions of enthalpy ($\%\xi_H$) and entropy ($\%\xi_{TS}$) in the dissolution process, eq 6, 7, and 8 were employed.[18,19]

$$\Delta G_d = \Delta H_d - T_m \cdot \Delta S_d \quad (6)$$

$$\%\xi_H = \frac{|\Delta H_d|}{|\Delta H_d| + |T_m \Delta S_d|} \times 100 \quad (7)$$

$$\%\xi_{TS} = \frac{|T_m \Delta S_d|}{|\Delta H_d| + |T_m \Delta S_d|} \times 100 \quad (8)$$

where T_m is the harmonic mean of the experimental temperatures from 278.15 to 328.15 K, namely, the value is 300.11 K.[20]

The values of thermodynamic parameters ΔH_d, ΔS_d, ΔG_d, $\%\xi_H$, and $\%\xi_{TS}$ for cytidine sulfate in pure water are listed in Table 1.

Table 1. Thermodynamic Parameters of Dissolution of Cytidine Sulfate in Pure Water

ΔH_d (kJ·mol^{-1})	ΔS_d (J·mol^{-1}·K)	ΔG_d (kJ·mol^{-1})	$\%\xi_H$	$\%\xi_{TS}$
21.68	28.68	13.07	71.58	28.42

As we can see in Table 1, the ΔH_d value is positive, indicating that the dissolution process in pure water is endothermic. It is coincident with the fact that the solubility of cytidine sulfate increases with rising temperature. The ΔS_d value is positive, suggesting that entropy is the driving force of the process. The ΔG_d value is positive, which indicates that the process is not spontaneous and the extra thermal compensation from the surrounding is indispensable for the dissolution to occur. The value of $\%\xi_H$ is greater than $\%\xi_{TS}$, which demonstrates that enthalpy is the main contributor to the Gibbs free energy during the dissolution process.

The solubility data of cytidine sulfate in water−ethanol binary solvents at 298.15 K are listed in Table S3. The relation between mole fraction solubility and the mole fraction of ethanol in binary solvents was correlated by the CNIBS/R-K equation as expressed in eq 9.[21,22] The calculated CNIBS/R-K solubility data ($x^{\text{CNIBS/R-K}}$) are also given in Table S3.

$$\ln x_1 = B_0 + B_1 x_2 + B_2 x_2^2 + B_3 x_2^3 + B_4 x_2^4 \quad (9)$$

https://doi.org/10.1021/acsomega.3c02501
ACS Omega 2023, 8, 25288−25294

where x_1 is the mole fraction solubility of cytidine sulfate; x_2 is the mole fraction of ethanol in binary solvents; and B_0, B_1, B_2, B_3, and B_4 are parameters obtained by nonlinear fitting.

The experimental solubility data and fitting curve are presented in Figure 4. The solubility of cytidine sulfate at 298.15 K decreases evidently as the mole fraction of ethanol in binary solvents rises. When the mass ratio of ethanol to water in a binary solvent reaches 10:3, the solubility is very low, approximately 0.7 g per kilogram of solvent. Therefore, antisolvent crystallization with ethanol as the antisolvent is a more suitable means of crystallization in terms of yield.

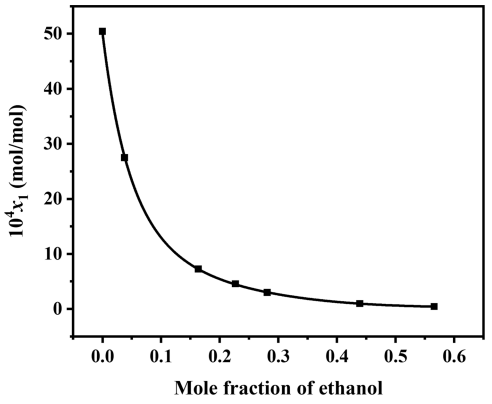

Figure 4. Mole fraction solubility of cytidine sulfate at 298.15 K in water−ethanol binary solvents correlated by the CNIBS/R-K equation.

The values of B_0, B_1, B_2, B_3, B_4, and R^2 and the root-mean-square deviations (RMSD) are listed in Table S4. From Figure 4 and Table S4, the experimental solubility data was successfully correlated by the CNIBS/R-K equation.

3.2. Comparison and Evaluation of Different Crystallization Methods. In this work, we investigated the effect of the crystallization method and operating parameter on the products. Cooling crystallization and antisolvent crystallization were chosen as the main methods. The cooling rate and the antisolvent feeding rate were used as the operating parameters that change the generation rate of supersaturation. The results are shown in Figures 5 and 6. The yield of cooling crystallization in pure water was 70−75%, while the yield of antisolvent crystallization could reach 92−97%. The product prepared by antisolvent crystallization had a higher packing density than cooling crystallization. The crystals of both methods had nearly blocky morphology and normal distributions in particle size. The mean particle size and packing density of the product prepared by cooling crystallization presented significant differences when changing the cooling rate: a lower cooling rate contributed to a larger particle size and a higher packing density, which is the ideal property for industrial crystallization. As to antisolvent crystallization, the ethanol feeding rate had little effect on the quality of crystals.

In order to optimize the process, the cooling−antisolvent coupling crystallization was developed combining the features of two methods. The cooling was conducted at a lower rate and stopped at the cloud point for crystals to grow. After cooling, ethanol was added to increase the yield. The results are shown in Figure 7. The product revealed the highest packing density, the largest mean particle size, and the most concentrated distribution. The yield reached 94−96%, which was similar to that of antisolvent crystallization. Therefore, the coupling method proved to be feasible for the industrial production of cytidine sulfate with good performance.

The particle size distribution and packing density data are listed in Table 2.

3.3. Product Characterization. *3.3.1. Structural Characterization.* The PXRD pattern of a crystalline material reflects its structure. It is practical to determine the crystallographic similarity of samples by pattern comparison.[23] PXRD patterns of samples prepared by three methods are shown in Figure 8a. From the patterns, it was found that the diffraction peaks appeared at almost the same diffraction angle (2θ), indicating that there was only one crystal form for cytidine sulfate in the research process.

Infrared spectroscopy is sensitive to the structure, conformation, and environment of organic compounds, making it a useful tool for crystal characterization.[23] As shown in Figure 8b, the sample exhibited O−H stretching vibration at 3311.11 cm^{-1}, N−H stretching vibration at 3130.87 cm^{-1}, C═O stretching vibration at 1725.93 cm^{-1}, C═C stretching vibration at 1668.27 cm^{-1}, and C−O stretching vibration at 1070.83 cm^{-1}. Furthermore, the three samples had nearly identical characteristic peaks and spectra, which further confirmed that the products had the same structure.

3.3.2. Thermal Analysis. TGA and DSC experiments were performed to investigate the thermal behavior of cytidine sulfate. From the TGA−DSC curve (Figure 9), there was no weight loss before 224 °C, meaning that there was no crystal

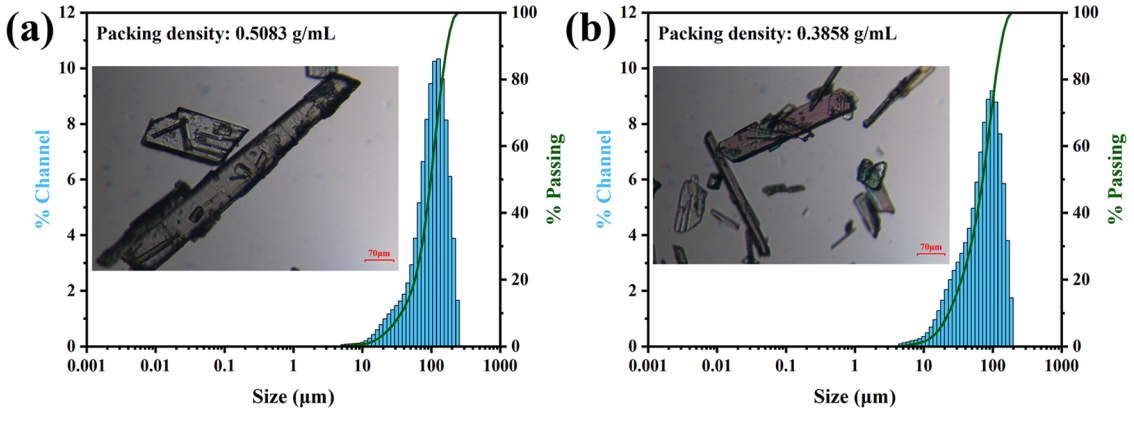

Figure 5. Particle size distribution of cytidine sulfate prepared by cooling crystallization at cooling rates of: (a) 0.5 K/min; and (b) 1.0 K/min.

https://doi.org/10.1021/acsomega.3c02501
ACS Omega 2023, 8, 25288−25294

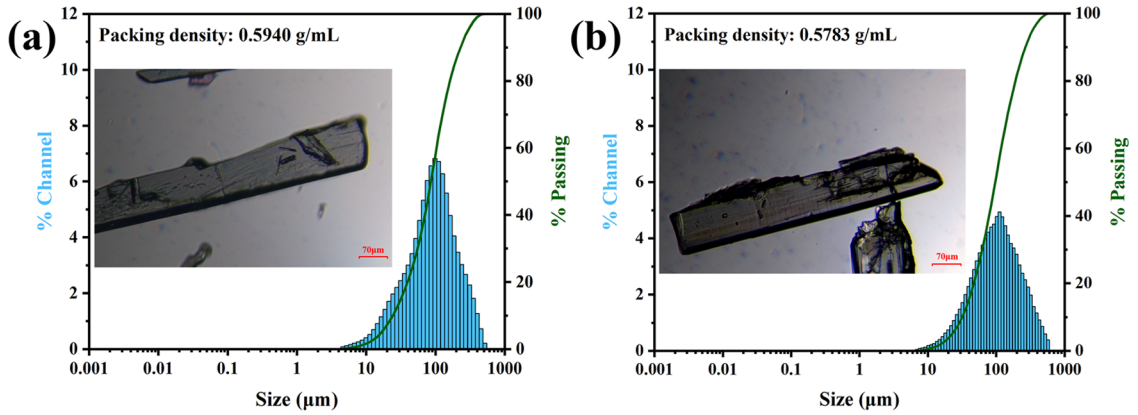

Figure 6. Particle size distribution of cytidine sulfate prepared by antisolvent crystallization at ethanol feeding rates of: (a) 0.5 mL/min; and (b) 1.0 mL/min.

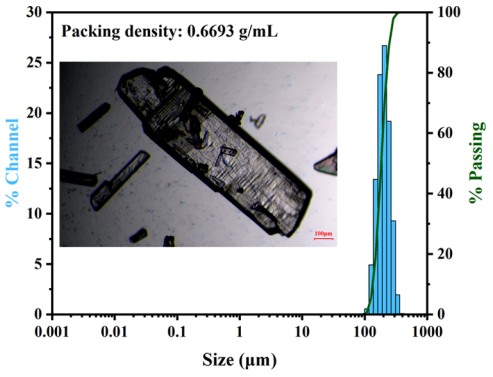

Figure 7. Particle size distribution of cytidine sulfate prepared by cooling−antisolvent coupling crystallization.

Table 2. Particle Size Distribution and Packing Density Data of Cytidine Sulfate Particles Prepared under Different Crystallization Conditions[a]

data item	CC0.5	CC1	AC0.5	AC1	C-ACC
D10 (μm)	41.5	25.9	27.3	30.1	161
D50 (μm)	112	81.0	97.5	95.4	216
D90 (μm)	192	148	261	273	291
D_d	1.34	1.51	2.40	2.55	0.60
PD (g/mL)	0.5083	0.3858	0.5940	0.5783	0.6693

[a]D_d: dispersion degree, D_d = (D90 − D10)/D50; PD, packing density; CC0.5, cooling crystallization at the rate of 0.5 K/min; CC1, cooling crystallization at the rate of 1.0 K/min; AC0.5, antisolvent crystallization at the feeding rate of 0.5 mL/min; AC1, antisolvent crystallization at the feeding rate of 1.0 mL/min; C-ACC, cooling−antisolvent coupling crystallization.

water in the unit cell and the sample was thermostable before decomposition. A major weight loss occurred around 226 °C, along with an obvious endothermic peak, which represented the decomposition process of the sample.

3.3.3. Humidity Stability Analysis. DVS analysis was performed to investigate the stability of the sample in the surrounding humidity. In the process, the sample was exposed to the programmed humidity at 25 °C and weighed to calculate the mass change. The results are shown in Figure 10. There were five desorption stages and four adsorption stages in the whole process. The mass of the sample changed within the range of ±0.01%. According to the results, the cytidine sulfate

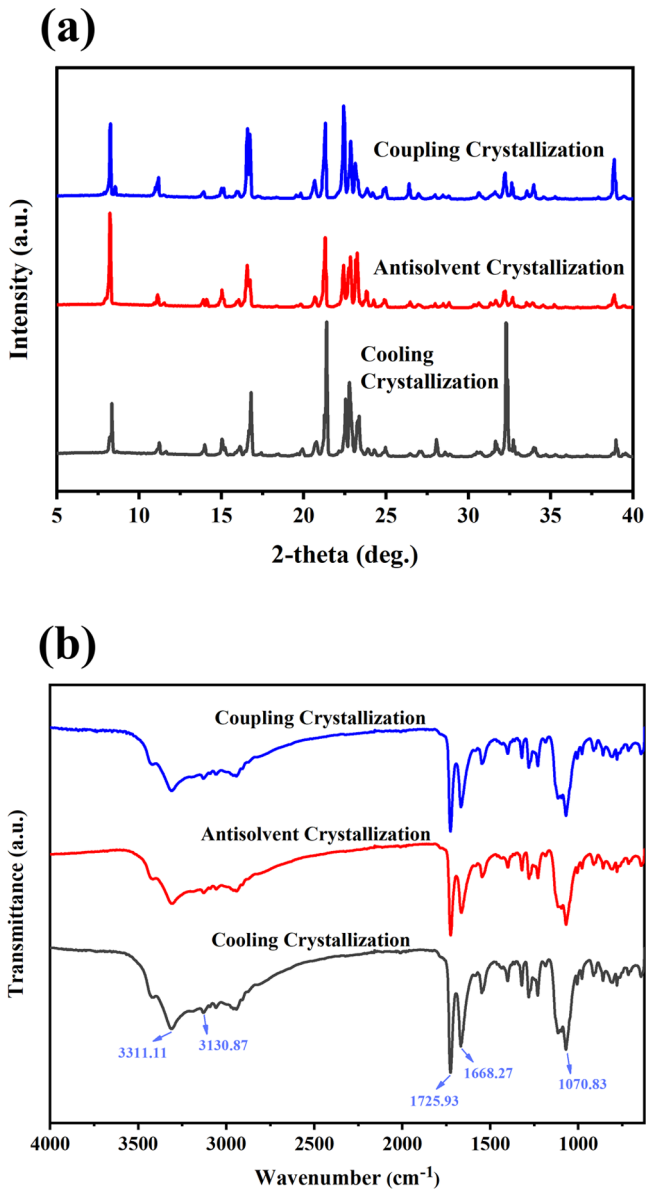

Figure 8. (a) PXRD patterns; (b) FTIR spectra comparison of cytidine sulfate prepared by three methods.

https://doi.org/10.1021/acsomega.3c02501
ACS Omega 2023, 8, 25288−25294

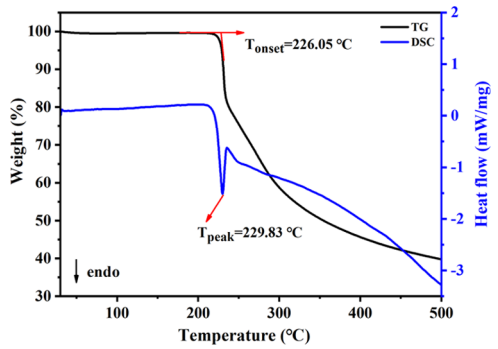

Figure 9. TGA−DSC curve of cytidine sulfate.

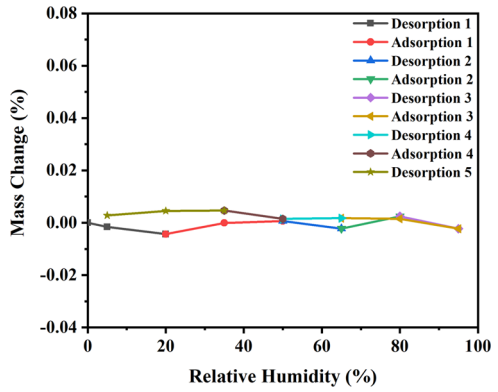

Figure 10. DVS curve of cytidine sulfate prepared by coupling crystallization.

product prepared by coupling crystallization is stable under the relative humidity of 0−95%.

4. CONCLUSIONS

The solubility of cytidine sulfate in pure water at different temperatures and in water−ethanol binary solvents at 298.15 K was measured, and the data were well-correlated by the modified Apelblat, van't Hoff, and CNIBS/R-K equations. It can be concluded that the solubility of cytidine sulfate increases with rising temperature in pure water and decreases with a rising ethanol ratio in binary solvents. The thermodynamic parameters of dissolution in pure water were calculated, proving an endothermic and nonspontaneous process driven by entropy.

The effect of crystallization method and operating parameter on the cytidine sulfate products was investigated. Cooling crystallization in pure water under a lower cooling rate tended to obtain crystals with a larger particle size and a more concentrated distribution. Antisolvent crystallization tended to obtain crystals with high yield and packing density. According to these features, the coupling method was successfully developed to produce cytidine sulfate with high quality.

It proved that cytidine sulfate prepared by the three methods has the same structure based on PXRD and FTIR characterization. The product obtained by coupling crystallization is thermostable before its decomposition at around 226 °C. The product is also stable under the relative humidity of 0−95%, facilitating storage and transport.

These findings provide a crystallization process suitable for the industrial production of cytidine sulfate. All of the work in the research may help with cytidine sulfate separation and purification.

■ ASSOCIATED CONTENT

Supporting Information

The Supporting Information is available free of charge at https://pubs.acs.org/doi/10.1021/acsomega.3c02501.

PXRD pattern and FTIR spectrum for the raw material of cytidine sulfate, experimental solubility of cytidine sulfate, and fitted parameters of the modified Apelblat equation and the CNIBS/R-K equation (PDF)

■ AUTHOR INFORMATION

Corresponding Author

Pengpeng Yang − *National Engineering Technique Research Center for Biotechnology, State Key Laboratory of Materials-Oriented Chemical Engineering, College of Biotechnology and Pharmaceutical Engineering, Nanjing Tech University, Nanjing 210009, China;* orcid.org/0000-0001-8722-9358; Email: yangpengpeng2013@126.com

Authors

Fan Leng − *National Engineering Technique Research Center for Biotechnology, State Key Laboratory of Materials-Oriented Chemical Engineering, College of Biotechnology and Pharmaceutical Engineering, Nanjing Tech University, Nanjing 210009, China*

Shuyang Zhou − *National Engineering Technique Research Center for Biotechnology, State Key Laboratory of Materials-Oriented Chemical Engineering, College of Biotechnology and Pharmaceutical Engineering, Nanjing Tech University, Nanjing 210009, China*

Shushu Li − *National Engineering Technique Research Center for Biotechnology, State Key Laboratory of Materials-Oriented Chemical Engineering, College of Biotechnology and Pharmaceutical Engineering, Nanjing Tech University, Nanjing 210009, China*

Mengjie Xu − *National Engineering Technique Research Center for Biotechnology, State Key Laboratory of Materials-Oriented Chemical Engineering, College of Biotechnology and Pharmaceutical Engineering, Nanjing Tech University, Nanjing 210009, China*

Keke Zhang − *Biology+ Joint Research Center, School of Chemical Engineering and Technology, Zhengzhou University, Zhengzhou 450001, China;* orcid.org/0000-0003-2576-6929

Ting Guo − *Jiangsu Academy of Agricultural Sciences, Nanjing 210014, China*

Tianpeng Chen − *National Engineering Technique Research Center for Biotechnology, State Key Laboratory of Materials-Oriented Chemical Engineering, College of Biotechnology and Pharmaceutical Engineering, Nanjing Tech University, Nanjing 210009, China*

Complete contact information is available at: https://pubs.acs.org/10.1021/acsomega.3c02501

Notes

The authors declare no competing financial interest.

■ ACKNOWLEDGMENTS

This work was supported by the National Key R&D Program of China 2022YFC2105400, the National Natural Science Foundation of China (22278217, 21908104), and the Jiangsu Provincial Key Research and Development Program (BE2019001).

REFERENCES

(1) Kumar, S.; Aakash, D.; Balasubramanian, N. A Review on Synthesis, Anticancer and Antiviral Potentials of Pyrimidine Derivatives. *Curr. Bioact. Compd.* **2019**, *15*, 289−303.

(2) Bezombes, C.; Laurent, G.; Jaffrezou, J.-P. Implication of raft microdomains in drug induced apoptosis. *Curr. Med. Chem. Anti-Cancer Agents* **2003**, *3*, 263−270.

(3) Gunji, H.; Kharbanda, S.; Kufe, D. Induction of internucleosomal DNA fragmentation in human myeloid leukemia cells by 1-beta-D-arabinofuranosylcytosine. *Cancer Res.* **1991**, *51*, 741−743.

(4) De Clercq, E. Anti-HIV drugs: 25 compounds approved within 25 years after the discovery of HIV. *Int. J. Antimicrob. Agents* **2009**, *33*, 307−320.

(5) Gopalsamuthiram, V.; Kadam, A. L.; Noble, J. K.; Snead, D. R.; Williams, C.; Jamison, T. F.; Senanayake, C.; Yadaw, A. K.; Roy, S.; Sirasani, G.; et al. Toward a Practical, Nonenzymatic Process for Investigational COVID-19 Antiviral Molnupiravir from Cytidine: Supply-Centered Synthesis. *Org. Process Res. Dev.* **2021**, *25*, 2679−2685.

(6) Iglesias, L. E.; Lewkowicz, E. S.; Medici, R.; Bianchi, P.; Iribarren, A. M. Biocatalytic approaches applied to the synthesis of nucleoside prodrugs. *Biotechnol. Adv.* **2015**, *33*, 412−434.

(7) Liu, H.; Yang, P.; Li, Z.; Wen, Q.; Li, X.; Zhu, C.; Jiao, P.; Zhuang, W.; Wu, J.; Ying, H. Thermodynamics, Characterization, and Polymorphic Transformation of 1,5-Pentanediamine Carbonate. *Ind. Eng. Chem. Res.* **2020**, *59*, 10185−10194.

(8) Wang, Y.; Yang, P.; Li, Z.; Fu, J.; Shi, Y.; Zhang, Y.; Zhang, K.; Zhuang, W.; Ying, H. Discovery and characterization of new crystal forms of bio-based nylon 4F salt. *CrystEngComm* **2022**, *24*, 5642−5652.

(9) Bard, B.; Martel, S.; Carrupt, P.-A. High throughput UV method for the estimation of thermodynamic solubility and the determination of the solubility in biorelevant media. *Eur. J. Pharm. Sci.* **2008**, *33*, 230−240.

(10) Wang, R. S.; Chen, C.; Yang, W. G.; Zhou, P.; Zhu, F.; Xu, H. H.; Hu, G. X.; Sun, W.; Shen, W. L.; Hu, Y. H. Solubility determination and thermodynamic characterization of orotic acid in twelve pure solvents and four binary mixed solvents. *J. Mol. Liq.* **2021**, *341*, No. 117335.

(11) Apelblat, A.; Manzurola, E. Solubilities of o-acetylsalicylic, 4-aminosalicylic, 3,5-dinitrosalicylic, and p-toluic acid, and magnesium-DL-aspartate in water from T = (278 to 348) K. *J. Chem. Thermodyn.* **1999**, *31*, 85−91.

(12) Anwer, M. K.; Mohammad, M.; Fatima, F.; Alshahrani, S. M.; Aldawsari, M. F.; Alalaiwe, A.; Al-Shdefat, R.; Shakeel, F. Solubility, solution thermodynamics and molecular interactions of osimertinib in some pharmaceutically useful solvents. *J. Mol. Liq.* **2019**, *284*, 53−58.

(13) Mullin, J. W. *Crystallization*, 4th ed.; Butterworth-Heinemann, 2001; pp 99.

(14) Grant, D. J. W.; Mehdizadeh, M.; Chow, A. H. L.; Fairbrother, J. E. Non-linear van't Hoff solubility-temperature plots and their pharmaceutical interpretation. *Int. J. Pharm.* **1984**, *18*, 25−38.

(15) Zhao, Y. H.; Hou, B. H.; Liu, C. H.; Ji, X. T.; Huang, Y. H.; Sui, J. C.; Liu, D.; Wang, N.; Hao, H. X. Mechanistic Study on the Effect of Magnetic Field on the Crystallization of Organic Small Molecules. *Ind. Eng. Chem. Res.* **2021**, *60*, 15741−15751.

(16) Qu, H.; Louhi-Kultanen, M.; Kallas, J. Solubility and stability of anhydrate/hydrate in solvent mixtures. *Int. J. Pharm.* **2006**, *321*, 101−107.

(17) Yang, P.; Peng, X.; Wang, S.; Li, D.; Li, M.; Jiao, P.; Zhuang, W.; Wu, J.; Wen, Q.; Ying, H. Crystal structure, thermodynamics, and crystallization of bio-based polyamide 56 salt. *CrystEngComm* **2020**, *22*, 3234−3241.

(18) Perlovich, G. L.; Kurkov, S. V.; Bauer-Brandl, A. Thermodynamics of solutions - II. Flurbiprofen and diflunisal as models for studying solvation of drug substances. *Eur. J. Pharm. Sci.* **2003**, *19*, 423−432.

(19) Perlovich, G. L.; Kurkov, S. V.; Kinchin, A. N.; Bauer-Brandl, A. Thermodynamics of solutions III: comparison of the solvation of (+)-naproxen with other NSAIDs. *Eur. J. Pharm. Biopharm.* **2004**, *57*, 411−420.

(20) Tian, Y.; Li, J.; Wu, B.; Zhang, Y.; Tang, H.; Li, Q. Determination and Modeling of the Solubility of 2,4-Dimethoxybenzoic Acid in Six Pure and Isopropanol + Ethyl Acetate Mixed Organic Solvents at Temperatures From (288.15 to 323.15) K. *J. Chem. Eng. Data* **2015**, *60*, 1098−1105.

(21) Acree, W. E., Jr. Mathematical representation of thermodynamic properties: Part 2. Derivation of the combined nearly ideal binary solvent (NIBS)/Redlich-Kister mathematical representation from a two-body and three-body interactional mixing model. *Thermochim. Acta* **1992**, *198*, 71−79.

(22) Yang, P.; Li, X.; Liu, H.; Li, Z.; Liu, J.; Zhuang, W.; Wu, J.; Ying, H. Thermodynamics, crystal structure, and characterization of a bio-based nylon 54 monomer. *CrystEngComm* **2019**, *21*, 7069−7077.

(23) Newman, A. W.; Byrn, S. R. Solid-state analysis of the active pharmaceutical ingredient in drug products. *Drug Discovery Today* **2003**, *8*, 898−905.

https://doi.org/10.1021/acsomega.3c02501
ACS Omega 2023, 8, 25288−25294